Anomalous Energy Transport to Rear Surface of Microdisks at High Laser Irradiances

N. A. Ebrahim, C. Joshi, D. M. Villeneuve, N. H. Burnett, and M. C. Richardson
Division of Physics, National Research Council of Canada, Ottawa K1A OR6, Canada
(Received 23 August 1979)

In CO_2-laser irradiation of thick microdisk foils, a significant fraction of the absorbed laser energy is found to be coupled to the rear surface. Moreover, $K\alpha$ and fast-ion emission has given, for the first time, direct evidence that the rear surface is subjected to considerable bombardment, by the transport of hot electrons around the target.

One of the most important problems in the studies of laser-produced plasmas is the transport of energy away from the region where the laser radiation is absorbed. Under conditions of collisionless absorption, laser energy is deposited into a hot-electron distribution at the critical surface. These electrons can distribute the energy in two ways. They can either transport the energy into the target interior and eventually form a thermal plasma, or they can accelerate fast ions via the ambipolar potential which is set up by the electrons attempting to leave the target. This partitioning of the absorbed energy, which is a sensitive function of possible transport inhibition into the target interior, is a topic of much contemporary diagnostic and theoretical interest.[1]

In this Letter we present experimental evidence which shows that in CO_2-laser irradiation of thick microdisk targets, a significant fraction of the absorbed energy is found coupled to the rear surface resulting in the formation of a hot plasma containing high-Z ionization states. Furthermore, $K\alpha$ emission and fast-ion generation from the rear surface of these targets suggests that a significant flux of hot electrons is incident on the rear surface. We propose that the rear-surface heating probably results from a combination of direct bombardment by hot electrons executing large-amplitude orbits in the electrostatic field of the target and propagation of the hot electrons through a laterally spreading plasma sheath. The strong implications that this lateral energy transport may have on the interpretation of high-irradiance laser interaction experiments are discussed.

The experiments have been performed with the COCO-II CO_2-laser (10.6-μm) system. In this series of experiments, laser pulses in the range 25–35 J and 1.3 ns full width at half maximum, were focused by an off-axis parabola onto thick microdisk Al foil targets approximately 500 μm in diameter. The foil thickness varied from 12.5 to 150 μm and target supports were either 10-μm glass stalks or 100-μm metallic wires. Unless otherwise specified, the results reported here were unaffected by the type of support used. The half-energy focal-spot diameter was 110 μm, yielding a maximum incident flux of 2×10^{14} W/cm^2. Approximately 90% of the total energy was contained within a 300-μm-diam region. Principal diagnostics (Fig. 1) included an extreme ultraviolet (XUV) spectroheliograph,[2] x-ray pinhole camera, Thomson parabolas,[3] time-of-flight ion probes, 180° focusing electron spectrographs, and rubidium acid phthalate crystal spectrograph. The asymptotic distribution of plasma energy was monitored with an array of twenty plasma calorimeters placed to cover as much of the solid angle as possible.

A typical x-ray pinhole image of plasma formed on a 500-μm-diam, 150-μm-thick Al microdisk is shown in Fig. 2(a). The x-ray pinhole camera recorded emission from x rays of photon energy in excess of 0.6 keV and had a spatial resolution of ~ 20 μm. It is seen that there is a very intense x-ray–emitting region, at the front surface, of ~ 300 μm in diameter. In addition, a narrow in-

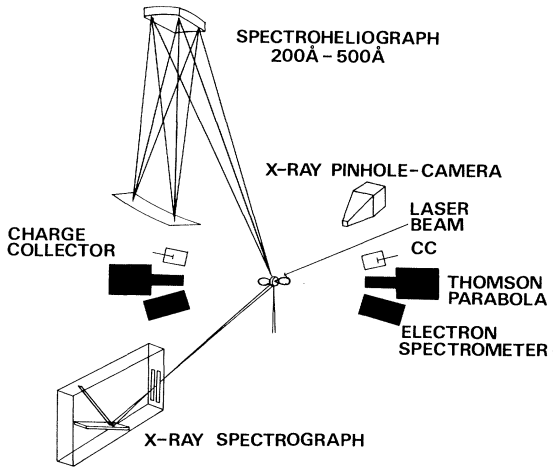

FIG. 1. Schematic diagram of the experimental arrangement.

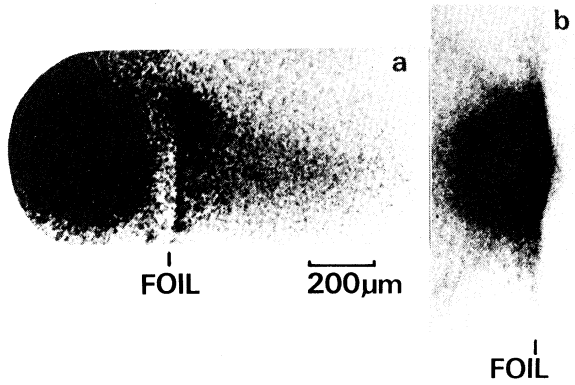

FIG. 2. X-ray pinhole image of (a) 150-μm-thick microdisk, (b) 10-mm-diam, 12.5-μm-thick Al foil.

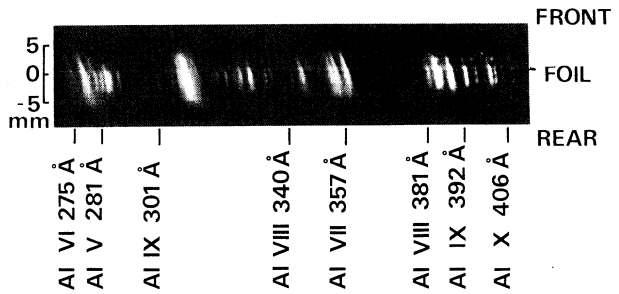

FIG. 3. Spectroheliogram of 12.5-μm-thick, 500-μm-diam Al target plasma.

tense x-ray region, consistent with a plasma temperature of the order of 100 eV, extends over much of the rear surface of the target. It is evident, simply on the basis of thermal capacity arguments, that bulk target heating to such temperatures cannot occur, and hence the rear plasma must result from a surface energy deposition. It is apparent from Fig. 2(b) that when the target diameter is increased to 10 mm, no significant plasma is present on the rear. It thus follows that the rear-surface plasma observed in Fig. 2(a) is a result of energy transport around, rather than through, the target.

The XUV radiation from the plasma was studied with a spectroheliograph which utilizes a toroidal grating to produce two-dimensional images of the plasma in discrete XUV lines (Fig. 3). Since the Doppler-broadening contributions are negligible, the spectral image quite accurately portrays the shape of the plasma in both directions. In the wavelength range of these spectra (~ 200–500 Å) the aluminum emission lines result from transitions between the $2s^2 2p^k$, $2s\,2p^{k+1}$, and $2p^{k+2}$ configurations within the ions of Al V through Al X, which are observed almost symmetrically front and back, implying that the temperatures at the front and rear are quite similar.

Similar front and back temperatures (of the order of 200 eV) were inferred from the thermal ion velocity distributions measured using charge collectors for microdisk targets, assuming an effective Z of 10, consistent with that deduced from the observed ionic species in the spectroheliograph data. Fast-ion emission was measured using Thomson parabolas in conjunction with cellulose nitrate film. The Thomson parabola in front of both 500-μm microdisks and 10-mm foils detected fast ions of charge species Al^{3+} through Al^{11+} and C^{1+} through C^{6+} as well as protons, these latter species evidently due to a contamination layer on the target surface. The maximum cutoff ion energy for aluminum was 2.5 MeV suggesting the emission of electrons up to the 200-keV range. In fact electrons in the energy range 50–600 keV have been detected by the electron spectrograph viewing the target front. Integrating over the measured angular distribution for a target mounted on a metallic stalk,[4] these suprathermal groups which escape the target field are found to contain almost 2% of the absorbed laser energy. The hot-electron temperature, however, is calculated in the isothermal approximation from the slope of the Al^{11+} energy distribution to be 20 keV. Significant numbers of fast ions were also detected in the backward direction from 500-μm microdisks, but not from 10-mm foils. For the microdisks, carbon species C^{+} through C^{5+} were observed, plus protons. The maximum carbon energies were ~ 0.6 MeV. No fast Al ions were detected, suggesting that for the back plasma only a thin surface layer of the order of a Debye length formed the fast blowoff. Observation of fast, high-Z ions at the back of the thick microdisks indicates the presence of a hot plasma in this region during the laser pulse since the hot electrons which accelerate them can exist only within the laser-pulse duration. Fast high-Z ions were observed from the rear side of 500-μm microdisks as thick as 150 μm. Since the hot-electron temperature estimated from the front fast-ion blowoff is of the order of 20 keV, it is difficult to accept that these rear ions could be accelerated by suprathermal electrons penetrating the bulk of the target. One is led to speculate that these ions must be accelerated by electrostatic fields set up by electrons which are emitted by the target.

It then follows that 10-mm targets of comparable thickness should greatly reduce the efficiency of fast-ion acceleration from the rear surface by modifying the distribution of the electrostatic field around the target.

The role of hot electrons in heating the rear surface of microdisks was further confirmed by direct observation of $K\alpha$ radiation which is essentially due to K-shell ionization by suprathermal electrons.[5] For microdisks as thick as 150 μm, $K\alpha$ radiation was observed from the rear surface and the intensity ratio front to back was measured to be 1.5 ± 0.2. The contribution to the front $K\alpha$ emission from radiation pumping was estimated to be small compared with the total observed front $K\alpha$ yield. Assuming the range of hot electrons to be much less than the target thickness, the ratio of $K\alpha$ intensities front and back should be a measure of the ratio of the hot-electron flux streaming into the target surfaces, provided that their energy distribution is the same.[5]

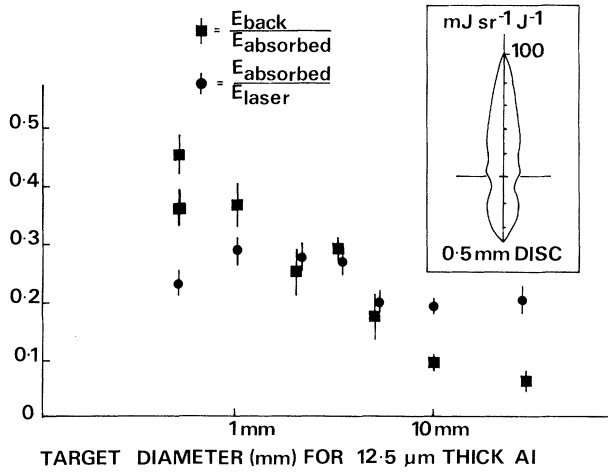

FIG. 4. (a) Integrated energy in the back hemisphere and the absorption fraction vs target diameter. The shaded portion shows the scatter in the data obtained during several experimental runs. (b) Polar plot of the energy distribution for a 500-μm target.

In order to determine the magnitude of energy transfer to the rear surface, the asymptotic plasma-energy distribution has been mapped for a series of 12.5-μm-thick foils of varying diameters between 500 μm and 10 mm. A typical polar plot of the actual energy distribution for a 500-μm-diam microdisk is shown as an inset to Fig. 4. It can be seen that the plasma energy is contained in two distinct lobes about the target, indicating that the observed plasma on the rear target surface is due largely to a surface deposition of energy rather than a manifestation of free convection. The ratio of the integrated energy in the back hemisphere to the absorbed energy is also shown in Fig. 4, as a function of target diameter. Up to 40% of the absorbed energy is found to be in the back 2π sr for a 500-μm-diam target. For larger-diameter targets the ion blowoff remained highly directional. Moreover, the absorption was found to be independent of the target diameter implying that the dynamic changes in the focal-spot area due to the refraction of the laser radiation in the plasma were not significant.

Fast-ion emission from the rear surface of thick microdisk targets strongly indicates the presence of an electrostatic field in the vicinity of this surface. The difference between the maximum front and back ion energies (2.5 to 0.6 MeV, respectively) and the lack of fast high-Z Al ions from the rear target surface suggests that the rear ions are accelerated from a thin surface charge layer by an electrostatic field which surrounds the whole target. In addition to the ambipolar plasma sheath in front of the target, one can expect the target as a whole to be surrounded by a space-charge sheath due to electrons making large-amplitude orbits from the target but confined by the target potential[6] and electrons escaping completely from the target field. The electron trajectories in this pure-electron-gas region ahead of the quasineutral plasma sheath will be determined by space-charge repulsion and the self-consistent magnetic field. Some of these electrons may follow trajectories of length comparable to the target diameter and thus reach the rear target surface, causing surface heating and also $K\alpha$ emission. The energy transported by orbiting electrons may be considerable since the target potential would be expected to trap most of the emitted electrons. Once a plasma sheath is formed around the target, lower-energy hot electrons with large angular momentum may be reflected in this region and also contribute to lateral energy transport.[7]

The precise role of the target potential on the effects reported here and its relation to target capacitance and stalk impedance must be further investigated. For microdisk targets the target potential probably will be limited by, but only weakly dependent on, the stalk impedance.[6] However, as the target diameter is increased, the capacitance of the target may become important in determining the target potential. In interpre-

ting burnthrough measurements on thin foils, intensity of the hard-x-ray spectra and the fraction of energy loss to fast-ion blowoff the role of lateral energy loss as described above must be considered. Detailed two-dimensional particle simulations are necessary to self-consistently determine the microscopic trajectories of hot electrons and their role in energy transport and fast-particle generation.

[1]William L. Kruer, Lawrence Livermore Laboratory

Report No. UCRL-82585, 1979 (unpublished).
[2]N. A. Ebrahim, M. C. Richardson, R. Fedosejevs, and U. Feldman, Appl. Phys. Lett. 35, 106 (1979).
[3]C. Joshi, M. C. Richardson, and G. D. Enright, Appl. Phys. Lett. 34, 625 (1979).
[4]C. Joshi and N. A. Ebrahim, Bull. Am. Phys. Soc. 24, 990 (1979).
[5]J. D. Hares, D. J. Kilkenny, M. H. Key, and J. G. Lunney, Phys. Rev. Lett. 42, 1216 (1979).
[6]Robert F. Benjamin, Gene H. McCall, and A. Wayne Ehler, Phys. Rev. Lett. 42, 890 (1979).
[7]J. R. Albritton, I. B. Bernstein, E. J. Valeo, and E. A. Williams, Phys. Rev. Lett. 39, 1536 (1977).

Phonon Anomalies and Electron-Lattice Coupling in Intermediate-Valence $Sm_{0.25}Y_{0.75}S$

H. Bilz, G. Güntherodt, W. Kleppmann, and W. Kress
Max-Planck-Institut für Festkörperforschung, D-7000 Stuttgart 80, Federal Republic of Germany
(Received 30 July 1979)

The electronic structure and the phonon dispersion curves of EuS, SmS, $Sm_{0.75}Y_{0.25}S$, and YS are analyzed. A five-parameter model is deduced which describes the phonon dispersion of $Sm_{0.75}Y_{0.25}S$ quite well. Two nearest-neighbor Sm-S forces and three deformabilities are introduced, two of which are attributed to virtual f-d transitions with dipolar- and "breathing"-type symmetry while the third is a quadrupolar-type sulfur deformability. The model suggests a strongly localized form of the microscopic theory.

Recently Mook *et al.*[1] have measured strong anomalies in the phonon dispersion curves of $Sm_{0.75}Y_{0.25}S$ which may be most likely related to the intermediate-valence state of $Sm_{1-x}Y_xS$ ($x > 0.15$).[2,3]

In this Letter we show that these anomalies can be described by a simple model which exhibits a clear radiation to excitations of Sm $4f$ electrons into d states of Sm, S, and Y. For this purpose we compare the electronic and vibrational properties of EuS, SmS, $Sm_{0.75}Y_{0.25}S$, and YS. The comparison suggests a five-parameter phonon model for $Sm_{0.75}Y_{0.25}S$. Two of these parameters may be interpreted as phonon self-energies due to virtual f-d transitions. The results suggest a specific form of the microscopic theory.

In Fig. 1 the essential properties of electrons and phonons of the aforementioned crystals are shown. While the upper part represents schematic diagrams of the valence and conduction bands,[4-6] the middle and lower parts of the figure show the calculated phonon dispersion curves in the (100) and (111) directions, respectively, except for $Sm_{0.75}Y_{0.25}S$ where guide-to-the-eye lines from experimental data[1] are shown. The calculations for EuS,[7] SmS,[8] and YS[9] reproduce the experimental data nearly within the limits of experimental error.[9,10]

In EuS the $4f$ states are in the lower part of the band gap of 2.3 eV and do not lead to any significant anomalies in the phonon dispersion curves, which are typical for an ionic semiconductor.[11]

As we proceed to SmS, the $4f$ level is shifted to the bottom of the conduction band and to the Fermi level E_F. In the optic branches a drastic lowering of the LO-TO splitting at Γ reflects the increase of the dielectric constant from $\epsilon_\infty = 4.7$ in EuS (Ref. 12) to $\epsilon_\infty \simeq 6.0$ in SmS,[13] although the band gap increases to 3 eV. This is caused by an enhanced Sm polarizability due to the lowered $4f$-$5d$ promotion energy, which corresponds to an increased dipolar phonon self-energy at Γ. An effect of similar magnitude occurs at the L point ("breathing" self-energy) which also reduces the bulk modulus by about 15%.[14] Thus, there is a clear indication of an incipient effect due to intermediate valence on the phonon dispersion of SmS.

The semiconductor-metal transition produces a drastic change in the phonon spectra as we go

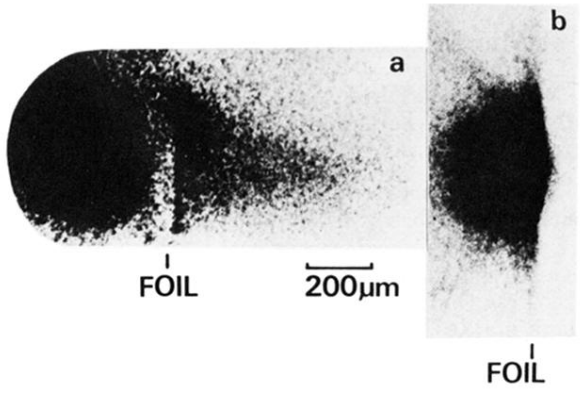

FIG. 2. X-ray pinhole image of (a) 150-μm-thick microdisk, (b) 10-mm-diam, 12.5-μm-thick Al foil.

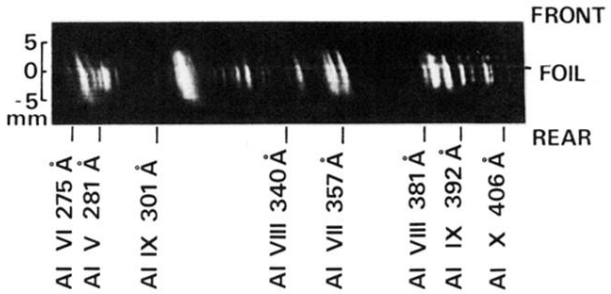

FIG. 3. Spectroheliogram of 12.5-μm-thick, 500-μm-diam Al target plasma.